⌘ *Author's Choice*

THE JOURNAL OF BIOLOGICAL CHEMISTRY VOL. 286, NO. 50, pp. 43172–43181, December 16, 2011

Picomolar Nitric Oxide Signals from Central Neurons Recorded Using Ultrasensitive Detector Cells*[S]

Received for publication, August 5, 2011, and in revised form, October 19, 2011 Published, JBC Papers in Press, October 20, 2011, DOI 10.1074/jbc.M111.289777

Katherine C. Wood, Andrew M. Batchelor, Katalin Bartus, Kathryn L. Harris, Giti Garthwaite, Jeffrey Vernon, and John Garthwaite[1]

From the Wolfson Institute for Biomedical Research, University College London, Gower Street, London WCIE 6BT, United Kingdom

Background: The biological actions of NO depend critically on its concentration, which is very difficult to measure.
Results: Recorded using the most sensitive detectors yet described, NO levels synthesized by activated brain neurons generally were in the picomolar range but varied regionally.
Conclusion: NO operates physiologically at the subnanomolar concentrations that selectively target its guanylyl cyclase-linked receptors.
Significance: Physiological NO levels are far lower than commonly supposed.

Nitric oxide (NO) is a widespread signaling molecule with potentially multifarious actions of relevance to health and disease. A fundamental determinant of how it acts is its concentration, but there remains a lack of coherent information on the patterns of NO release from its sources, such as neurons or endothelial cells, in either normal or pathological conditions. We have used detector cells having the highest recorded NO sensitivity to monitor NO release from brain tissue quantitatively and in real time. Stimulation of NMDA receptors, which are coupled to activation of neuronal NO synthase, routinely generated NO signals from neurons in cerebellar slices. The average computed peak NO concentrations varied across the anatomical layers of the cerebellum, from 12 to 130 pM. The mean value found in the hippocampus was 200 pM. Much variation in the amplitudes recorded by individual detector cells was observed, this being attributable to their location at variable distances from the NO sources. From fits to the data, the NO concentrations at the source surfaces were 120 pM to 1.4 nM, and the underlying rates of NO generation were 36–350 nM/s, depending on area. Our measurements are 4–5 orders of magnitude lower than reported by some electrode recordings in cerebellum or hippocampus. In return, they establish coherence between the NO concentrations able to elicit physiological responses in target cells through guanylyl cyclase-linked NO receptors, the concentrations that neuronal NO synthase is predicted to generate locally, and the concentrations that neurons actually produce.

Nitric oxide (NO) is one of the most widely used transmitters in mammals, playing fundamental roles in the normal functioning of the nervous, cardiovascular, urogenital, digestive, and other systems (1–3). Physiologically, NO signals are normally generated by neuronal NO synthase (nNOS)[2] or endothelial NO synthase and are transduced in target cells through specialized receptors possessing an intrinsic guanylyl cyclase (GC) domain, resulting in cGMP accumulation (4, 5). Beyond this, details of its functioning remain uncertain. Unlike conventional transmitters, NO is not constrained by cellular membranes and so diffuses in three dimensions from where it is synthesized. Among the many unknowns are the patterns of NO formation by different sources (*e.g.* neurons or endothelial cells) and how far it is able to spread in active concentrations (and what an "active concentration" actually is), the molecular targets other than GC-coupled receptors available to NO, and how it is inactivated. Moreover, supposed abnormalities in NO levels have been implicated in many disease states but what distinguishes the physiological from the pathophysiological in terms of the amount, duration, or pattern of NO formation remains undefined.

Progress in these key issues requires accurate measurement of NO release from its sources under different conditions. Numerous attempts have been made using electrodes of various designs for this purpose but the outcome has been an impossibly large spread of values. In the brain, for instance, estimates of the NO concentration after stimulation span over 4 orders of magnitude, from the picomolar to the micromolar, with a similar variability applying to other tissues (reviewed in Ref. 6). Other approaches indicating concentrations of 0.1 to 4 nM (7–10) would favor the lowest extreme of the spectrum of electrode measurements or below. Knowledge of the true range impacts directly on how NO might be acting: at the low end (nM and below) NO selectively stimulates GC-coupled receptors, whereas as its concentration increases (10–100 nM range), it can inhibit mitochondrial respiration by competing with O_2 for

* This work was supported by Programme Grant 081512 from The Wellcome Trust.
⌘ *Author's Choice*—Final version full access.
[S] The on-line version of this article (available at http://www.jbc.org) contains supplemental Methods, Figs. 1–5, Movies 1 and 2, and additional references.
[1] To whom correspondence should be addressed: Wolfson Institute for Biomedical Research, University College London, Gower Street, London WCIE 6BT, UK. Tel.: 44-20-7679-6694; Fax: 44-20-7209-0470; E-mail: john.garthwaite@ucl.ac.uk.

[2] The abbreviations used are: nNOS, neuronal NO synthase; CPTIO, 2-(4-carboxyphenyl)-4,4,5,5-tetramethylimidazoline-1-oxyl-3-oxide; GC, guanylyl cyclase; ODQ, 1*H*-[1,2,4]oxadiazolo[4,3-*a*]quinoxalin-1-one; PDE5, phosphodiesterase-5; PAPA/NO, (*Z*)-1-[*N*-(3-ammoniopropyl)-*N*-(*n*-propyl)amino]diazen-1-ium-1,2-diolate]; EGFP, enhanced GFP; TBST, Tris-buffered saline containing 0.1% Triton X-100; c[NO], computed NO concentration.

binding to cytochrome *c* oxidase and, at near-micromolar levels, it can undergo various chemical reactions leading secondarily to covalent protein modifications (6, 11).

By analyzing NO signal transduction through GC-coupled receptors (12) and the subsequent real-time imaging of cellular NO-evoked cGMP signals in cells expressing different amounts of receptor and cGMP-degrading phosphodiesterase activity (13), it has become evident that, by virtue of this pathway, cells are able to detect astonishingly low NO concentrations (low pM) even when the exposure is fleeting (subsecond). The results prompted the elaboration of a kinetic model that accurately simulated the cellular cGMP responses to transient or sustained NO concentrations. The opportunity then arose to exploit receptor-containing cells as detectors of endogenous NO, offering the benefits of unsurpassed sensitivity, selectivity, and dynamism. We report here the use of such cells for quantitatively recording NO signals generated by central neurons on stimulation of NMDA receptors, the prototypical receptors coupled to nNOS activation in the brain (14).

EXPERIMENTAL PROCEDURES

Materials—1*H*-[1,2,4]oxadiazolo[4,3-*a*]quinoxalin-1-one (ODQ) was from Tocris Bioscience (Bristol, UK); 2-(4-carboxyphenyl)-4,4,5,5-tetramethylimidazoline-1-oxyl-3-oxide (CPTIO), 8-bromo-cGMP, *N*-methyl-D-aspartate (NMDA), D-2-amino-5-phosphonopentanoic acid, N-nitro-L-arginine, superoxide dismutase and tetrodotoxin were from Sigma-Aldrich; fluorescein was from Millipore (Watford, UK); (*Z*)-1-[*N*-(3-ammoniopropyl)-*N*-(*n*-propyl)amino]diazen-1-ium-1,2-diolate] (PAPA/NO) was from Enzo Life Sciences (Exeter, UK); bicuculline methochloride was from Ascent Scientific (Bristol, UK). Common laboratory chemicals were from Sigma-Aldrich. Computer modeling used Mathcad (version 14, Parametric Technology Corp., Needham, MA).

NO Detector Cells—HEK293T cells expressing NO-activated GC and phosphodiesterase-5 (PDE5), previously called $GC_{high}PDE5_{low}$ cells (13), were provided by Professor Doris Koesling (Ruhr-Universität Bochum, Bochum) and maintained as done previously (13). The cells growing on coverslips were either infected with an adenoviral vector expressing δ-FlincG (13, 15) or were transfected (using FuGENE 6, Roche Applied Science) with a cDNA plasmid as per the manufacturer's instructions and were used 2–4 days later. For the plasmid, the cDNA for δ-FlincG was retrieved from an adenoviral supernatant. Approximately 850 surplus nucleotides beyond the stop codon were deleted, and EGFP codon 215 was restored to arginine (from cysteine). This version of δ-FlincG was substituted for the EGFP sequence in pEGFP-C1 (Takara Bio Europe/Clontech, Saint-Germain-en-Laye, France).

Brain Slices—Rats (either gender) aged either 10 days (for cerebellum) or 8 days (for hippocampus) were killed by cervical dislocation and decapitation in accordance with UK Home Office regulations. The tissue was removed and placed in ice-cold artificial cerebrospinal fluid containing the following: NaCl (120 mM); KCl (2 mM); $NaHCO_3$ (26 mM); KH_2PO_4 (1.18 mM); $MgSO_4$ (1.19 mM); glucose (11 mM), and $CaCl_2$ (2 mM), bubbled with 95% O_2, 5%CO_2. Using a vibratome (Intracel 1000 plus, Intracel Ltd., Royston, UK), slices (200-μm thick) were cut from the cerebellar vermis (sagittal plane) or the hippocampus (transverse plane) and transferred to a recovery chamber at 37 °C, which was subsequently allowed to cool to room temperature (≈22 °C).

Imaging—A coverslip with adherent NO detector cells was placed in a small chamber (500-μl volume) mounted on an inverted microscope (Zeiss Axiovert 135TV, Carl Zeiss Ltd., Welwyn Garden City, UK). After being allowed to recover for at least 30 min, a brain slice was positioned on top of the coverslip and held steady by a harp-type slice anchor (weight, 0.4 g). The chamber was continuously superfused (1.5 ml/min) with warm (37 °C) solution containing the following: NaCl (140 mM), KCl (2 mM), KH_2PO_4 (1.18 mM), glucose (5.5 mM), HEPES (10 mM), and $CaCl_2$ (1.5 mM), pH 7.4, osmolality 285–290 mosmol kg^{-1}. When equilibrated with pure O_2, the solution was supplemented with superoxide dismutase (100 units/ml). Tetrodotoxin (1 μM) was included in all hippocampal slice experiments to avoid circuit-based activity. Imaging was performed as described previously (13) using a 20× air objective (numerical aperture, 0.5, Carl Zeiss), an exposure time of 40 ms, and a nominal frame rate of 0.7 Hz. Drugs were administered by superfusion; fluorescein (50 pM) was delivered at the end of each experiment to estimate the delay resulting from the dead space of the perfusion line, for which traces were corrected. Fluorescence measurements were background-corrected and displayed as the change in intensity relative to baseline divided by the baseline intensity ($\Delta F/F_0$). As appropriate, traces were corrected for NO-independent, post-NMDA undershoots (supplemental Fig. 1) and baseline drift (13) in Origin (version 8.1, OriginLab Corp., Northampton, MA). Individual detector cells were classed as responders to NMDA if a peak of fluorescence more than 2 S.D. above the baseline fluorescence was observed within a 135-s window starting at the beginning of the NMDA application. Results are given as means ± S.E. unless otherwise stated. Each experiment was carried out on a separate brain slice and was conducted at least twice to ensure that the results were repeatable; *n* values refer to the number of detector cells. Gaps in the illustrated records correspond to periods of 1–3 min during which recording was suspended.

Immunohistochemistry—Cerebellar and hippocampal slices were incubated in the recovery chamber for 1–1.5 h and then fixed with 1% paraformaldehyde for 1 h at room temperature, washed with 0.1 M phosphate buffer for 1 h (with three changes), incubated for 5 min with Tris-buffered saline containing 0.1% Triton X-100 (TBST), and then blocked with 10% donkey serum in TBST for 1 h at room temperature. The slices were then incubated with rabbit anti-nNOS (1:700; Invitrogen) in TBST for 2 h at room temperature and then for 2 days at 4 °C. Mouse anti-calbindin (1:5000; Sigma-Aldrich) was added for 24 h at 4 °C. Afterward, the slices were washed in TBST for 6–7 h with three changes and then incubated overnight at 4 °C with secondary antibodies (anti-rabbit Alexa Fluor 488, 1:1000 and anti-mouse Alexa Fluor 568, 1:500; both Invitrogen). After further washing for 6–7 h in TBST, slices were incubated with the nuclear stain TO-PRO-3 (1:50,000; Invitrogen) for 5 min before being mounted in Vectashield mounting medium (Vector Laboratories, Peterborough, UK). Secure seal adhesive spacers (Invitrogen) were used to prevent the coverslip compressing

the slices. Z-images through the entire slice thickness were captured at different step sizes using a confocal microscope (SP1, Leica Microsystems Ltd., Milton Keynes, UK). For staining sections, 10-day-old rat cerebella were divided in two, immersed in 1% paraformaldehyde for 2 h at 4 °C, washed for 1.5 h with 0.1 M phosphate buffer, and sectioned (10 μm) on a cryostat. Sections were blocked as described above, and primary antibodies were applied overnight at 4 °C. Sections were washed with TBST for 40 min (with four changes) and incubated with secondary antibodies for 1 h at room temperature. The TBST washes were repeated, and TO-PRO-3 (1:30,000) was applied as above.

Quantification of NO Signals—The NO profiles underlying the changes in δ-FlincG fluorescence in the detector cells were computed on the basis of the NO receptor, PDE5, and δ-FlincG kinetics described previously (13). Full details of the methods, together with the modeling of NO diffusion in and around the detector cells and the derivation of the tissue NO concentrations and NO synthesis rates are provided in the supplemental Methods. Annotated Mathcad worksheets are available upon request.

RESULTS

Recording NO Release from Cerebellar Slices Using Detector Cells—The experiments used thin brain slices (200-μm thick) positioned on top of NO-detecting HEK 293T cells stably expressing NO-activated GC and PDE5 (16) together with the fluorescent cGMP biosensor δ-FlincG (15) expressed transiently (Fig. 1*A*). Most studies used slices of the developing rat cerebellum (10 days old), which was selected because the neurons in this region reside in distinct layers (Fig. 1*B*) and it contains a high level of nNOS (17), whose activity is stimulated by the influx of Ca^{2+} occurring on stimulation of NMDA receptors (14), a response that is highest in the developing tissue (18). Superfusion of NMDA (30 μM for 45 s) led to an obvious increase in fluorescence in many of the underlying NO detector cells (Fig. 1, *D* and *E*; supplemental Movie 1). The absolute response amplitudes varied across the field of cells, and on washing out the NMDA, the fluorescence recovered (Fig. 1, *G* and *H*). To calibrate the effect of NMDA, it was necessary to measure the maximum response of the detector cells. This was achieved by superfusing the NO donor PAPA/NO in a high enough concentration (5 μM for 1.5 min) to achieve supramaximal stimulation in the face of rapid NO consumption by the overlying slice (19). In some detector cells, PAPA/NO generated a response where none was visible previously with NMDA, whereas in others, the peak amplitudes with PAPA/NO or NMDA were comparable (Fig. 1, *F–H*; supplemental Movie 1). The fluorescent responses of the detector cells to different patterns of NO delivery (in known concentration) can be accurately simulated by a computer model that incorporates the kinetics of the NO receptor and PDE5 limbs of the transduction pathway (12, 13, 20). With this model, the profile of the NO concentration reaching the cells after NMDA stimulation could be computed from the fluorescence data (supplemental Methods). Applying the method to the two sample cells in the experiment illustrated in Fig. 1, *C–F*, gave computed NO concentrations (c[NO]) of 0.5 nM and 28 pM (Fig. 1, *G* and *H*, *insets*).

With increasing NMDA concentrations (3–100 μM), the detector cells responded accordingly and with a latency that became progressively shorter (Fig. 1*I*). From the mean detector cell responses, the c[NO] rose from undetectable up to 480 pM at 100 μM NMDA (Fig. 1*J*). Much variation was again evident at the level of single detector cells, but the concentration-response curves for those giving high and low amplitude signals were not significantly different from each other or from the population as a whole ($EC_{50} \approx 30$ μM; Fig. 1*K*), so the variation could not be explained by NMDA having a different potency in different subregions of the cerebellum. An EC_{50} concentration (30 μM) was chosen for the following experiments.

Pharmacology of NMDA-evoked NO Release—The detector cell responses to NMDA, but not to PAPA/NO, were abolished by the NO synthase inhibitor, L-nitroarginine (Fig. 2*A*). The NO receptor blocker ODQ also inhibited the NMDA-evoked response, but the cells still responded to the slowly permeating cGMP derivative, 8-bromo-cGMP (Fig. 2*B*), confirming that the detector cell responses were NO receptor-mediated. The NMDA antagonist D-2-amino-5-phosphonopentanoic acid (Fig. 2*C*) was also inhibitory, but the response was unchanged in the presence of tetrodotoxin (Fig. 2*D*), which blocks voltage-gated sodium channels and, hence, circuit-based neuronal excitation, or of bicuculline (Fig. 2*E*), which blocks $GABA_A$ receptors. These results verify that the detector cells are responding to NO generated on NMDA receptor activation and further suggest that NMDA is acting directly and in a manner that is not significantly affected by its ability to stimulate the release of GABA from inhibitory interneurons (21). In all of these tests, the average peak c[NO] was in the range of 100–150 pM (Fig. 2, *A–E*, *insets*).

NO Release from Cerebellar Subregions—The cerebellar cortex contains relatively few neuronal cell types: at the age used (10 days after birth) the outermost layer, the external granule cell layer, is a germinal zone containing granule cell progenitors. Differentiated granule cells are found in the innermost layer (internal granule cell layer), above which lie the Purkinje cell bodies (Purkinje cell layer) and the molecular layer, which consists largely of the excitatory axons of granule cells and the Purkinje cell dendrites and inhibitory interneurons onto which they synapse (Fig. 3, *A* and *B*). Immunocytochemistry for nNOS protein in sections of cerebellum revealed the brightest staining to be in the molecular layer, followed by the internal granule cell layer (Fig. 3, *A–C*). Immunoreactivity in the Purkinje cell layer was weak (Purkinje cells were unstained), and there was only very sparse staining in the external granule cell layer. This distribution is broadly consistent with observations made on rat cerebellum at other developmental ages (22).

When the NO detector cells were grouped according to their location relative to the overlying cerebellar slices, clear variation on exposure to NMDA was seen. The Purkinje layer could not be defined unambiguously in brightfield images (Fig. 1*B*) and is of similar width to the detector cells, so the region between the two granule cell layers was treated as a single layer (molecular plus Purkinje cell layer). Detector cells lying just outside the slices never responded to NMDA (Fig. 3, *D* and *E*; see also Fig. 1, *B–E*). In the external granule cell layer, the average response amplitude was low, corresponding to a peak

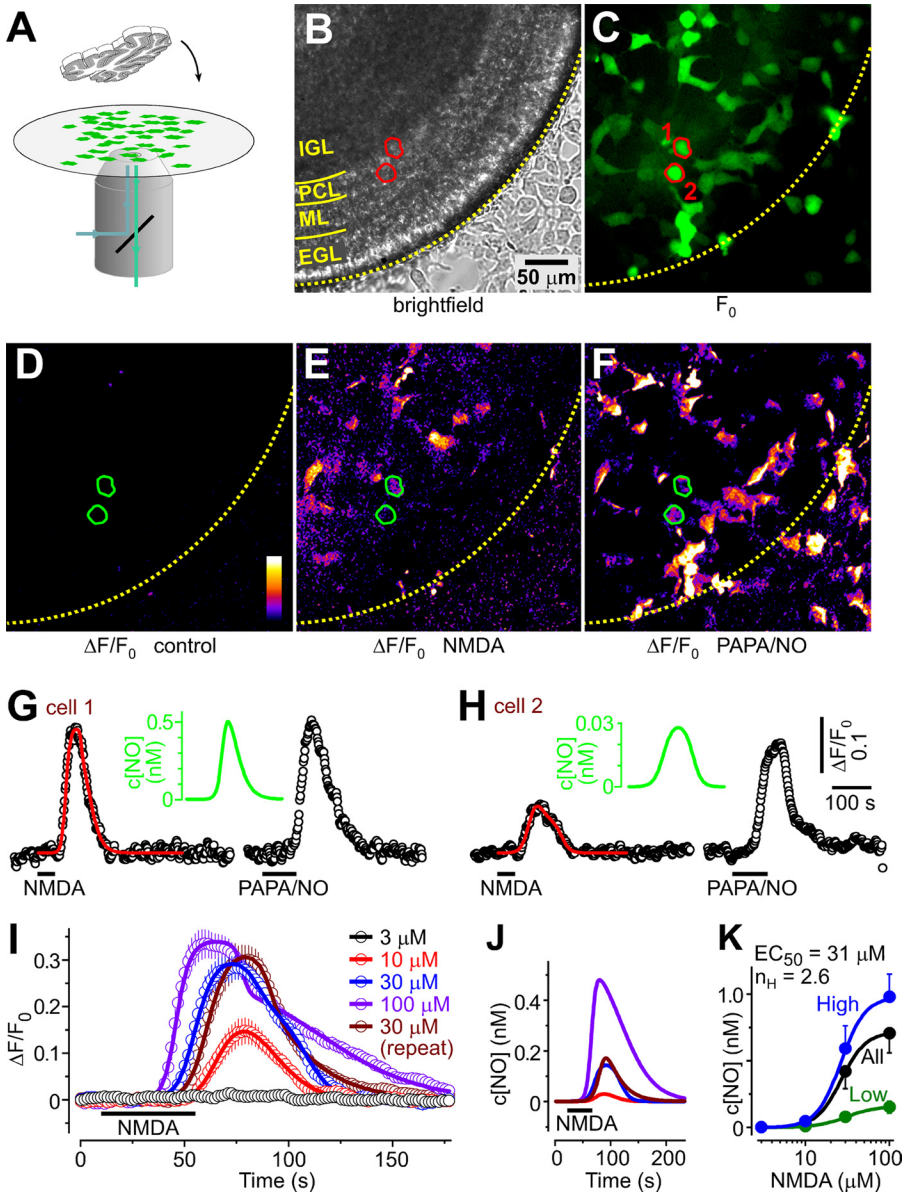

FIGURE 1. **Imaging NO release from cerebellar slices on exposure to NMDA.** *A*, schematic showing NO detector cells (*green*) on a glass coverslip. A 200-μm-thick cerebellar slice was wedged on top and imaging was from below. *B*, brightfield image of a cerebellar slice (*IGL*, internal granule cell layer; *PCL*, Purkinje cell layer; *ML*, molecular layer; *EGL*, external granule cell layer). *C*, fluorescent image of underlying detector cells. *D–F*, images of $\Delta F/F_0$ before (*D*) and at the peak of the response (*E*) to 30 μM NMDA applied for 45 s and of 5 μM PAPA/NO applied for 90 s (*F*). Responses in two sample cells outlined in *red* in *B* and *C* and *green* in *D–F* are plotted in *G* and *H*, with the NO profiles computed from fits to the data (*red lines*) given in the *insets*. *I–K*, effect of increasing the NMDA concentration (3–100 μM) on $\Delta F/F_0$ (*I*) and c[NO] (*J*). NMDA was superfused for 45 s in ascending concentrations at 15 min intervals, 30 μM being repeated at the end. Lines (*I*) fit the c[NO] profiles to the data. *K*, concentration response curves for c[NO]. A logistic fit to values for all the detector cells in this experiment (*All*; $n = 21$) gave the stated EC_{50} and Hill slope (n_H). When subdivided into *High* (> 0.5 nM) and *Low* (<0.5 nM) responders based on the peak c[NO] at 100 μM NMDA, EC_{50} and Hill slope values were 30 ± 5 μM and 2.7 ± 1.8 (*High*; $n = 14$), and 40 ± 22 μM and 2.1 ± 1.6 (*Low*; $n = 7$), respectively, neither of which differs significantly ($p = 0.7$ and 0.6).

c[NO] of only 12 pM (Fig. 3, *E*, *inset*, and *H*), whereas the molecular/Purkinje cell and internal granule cell layers all responded more robustly, giving mean peak c[NO] values of 60 and 130 pM, respectively (Fig. 3, *D*, *E*, and *H*). Throughout the tissue, some detector cells gave no discernible response to NMDA; these were more prevalent (23/42 or 55%) in the external granule cell layer than elsewhere: 12/62 (19%) in the molecular/Purkinje cell layer and 15/68 (22%) in the internal granule cell layer. When only the responders were analyzed (Fig. 3*G*), the mean peak c[NO] in the three layers was higher (Fig. 3*H*), but the difference between the layers was maintained (25, 115, and 277 pM). The amplitudes of responses to PAPA/NO were similar regardless of their position (Fig. 3*F*), although the latency-to-peak increased with distance from the slice edge (see also supplemental Movie 1).

Localization of NO Sources and Detectors—The results above indicate that global NMDA receptor stimulation does not generate a uniform "cloud" of NO within the cerebellum (*cf.* Ref. 7), that the local NO concentrations detected are generally in the subnanomolar range, and that immeasurably small amounts of NO escape the edge of the tissue. To examine further the extent to which NO reaching the detectors is affected by the mixing of

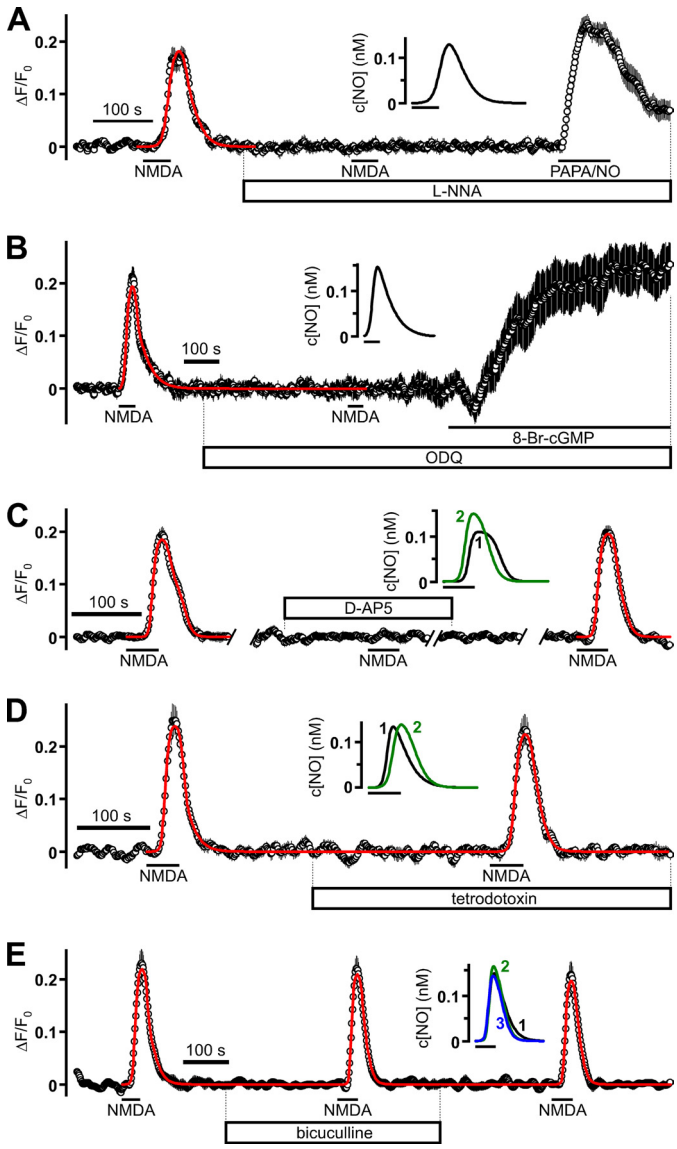

FIGURE 2. **Pharmacology of NMDA-induced NO release from cerebellar slices.** Data show $\Delta F/F_0$ in detector cells (n = 12–22) on applying 30 μM NMDA (*black bars*) in the absence and presence of 30 μM L-nitroarginine (*L-NNA*; *A*), 10 μM ODQ (*B*), 50 μM D-2-amino-5-phosphonopentanoic acid (*D-AP5*; *C*), 1 μM tetrodotoxin (*D*), and 30 μM bicuculline (*E*); *D* and *E* are from the same experiment. PAPA/NO (5 μM) and 8-bromo-cGMP (*8-Br-cGMP*, 1 mM) were added as controls at the end in *A* and *B*, respectively. *Insets*, c[NO] profiles, numbered in chronological order; their fits to the experimental data are shown by *red lines* in the main panels.

NO from different localities, a high concentration (250 μM) of the NO scavenger CPTIO was superfused. Rather than becoming smaller, the average detector cell responses increased (Fig. 4*A*). Where evident, this increase could be largely explained by time-dependent changes in the detector cell PDE5 activity: the second response to NMDA is smaller than the first because NO from the first application, through cGMP, results in activation of PDE5 in the detector cells (Fig. 4*C*). During the time that CPTIO is allowed to equilibrate, the proportion of activated PDE5 declines, leading to an increase in the response to the third NMDA exposure relative to the second. Thus, the data are consistent with the NO profile being unaltered in the presence of CPTIO (Fig. 4, *B* and *C*). From the reaction kinetics (23), 250 μM CPTIO consumes NO at a rate of 4 s^{-1}, imposing on NO a half-life of 170 ms. With no other NO scavenging, a lack of effect of CPTIO implies that the sources and detectors are close together (supplemental Fig. 4*B*). However, cerebellar tissue consumes NO at a very high rate (19), such that at subnanomolar concentrations, NO would be inactivated at a rate of 150 s^{-1} (half-life = 5 ms). Presumably, this rate predominates so that, superimposed on it, NO scavenging by CPTIO becomes negligible. The steep NO concentration gradient that this high rate of consumption imposes around a source suggests, moreover, that the source-detector separation is likely to be in low μm range (supplemental Fig. 4, *B* and *C*). In liver, aorta, and a carcinoma cell line, the rate of inactivation of NO, and hence its diffusion distance, depends on the concentration of O_2 (24–26). Switching between superfusion solutions equilibrated with air (21% O_2) or with pure O_2, however, had no consistent effect on the amplitude or shape of the detector cell responses to NMDA (Fig. 4, *D* and *E*). In one respect, this result was surprising because from the behavior of the purified enzyme, nNOS activity is expected to be highly O_2-dependent (27). Possibly, increased NO generation at high O_2 concentrations is balanced by increased NO consumption.

Heterogeneity of Recorded NO Signals—We have alluded already to the variation in amplitude of c[NO] profiles recorded by different detector cells even when they are situated close to each other (*e.g.* Fig. 1, *D–H*). This heterogeneity could not be attributed to a variable sensitivity of single detector cells to NO (supplemental Fig. 5) and was investigated further by analyzing individual responses to NMDA in five experiments. In the example illustrated (Fig. 5*A*), the peak c[NO] varied from 16 pM to just over 1 nM, with the higher values being found in the internal granule cell layer, and there were instances of detectors giving moderate-to-high amplitude responses located close to ones that were unresponsive (although they responded to PAPA/NO). The c[NO] values for all the "responder" cells (n = 95) were not normally distributed ($p = 2 \times 10^{-15}$ with the Shapiro-Wilk test) and a frequency count after sorting them into 10 pM bins showed a highly positively skewed distribution (Fig. 5*B*). The measurements conformed to a lognormal distribution, irrespective of the cerebellar layer under which the detectors were located, as shown by the linear fits in lognormal probability plots (Fig. 5*B*, *inset*). The median c[NO] values varied from 21 pM in the external granule cell layer to 171 pM in the internal granule cell layer, with all layers differing significantly from each other (Table 1).

Attempts were made to try to identify the sources of NO located immediately above the detector cells using post hoc nNOS immunohistochemistry, but the tissue distortion occurring on fixation prohibited this approach. Nevertheless, whole-mount nNOS immunostaining of incubated cerebellar slices showed a spectrum of nNOS-positive structures at the slice surface, ranging from small puncta to fibers to cell bodies (Fig. 5, *C* and *D*; supplemental Movie 2). By following these structures through into deeper regions, they were mostly seen to be the cell bodies and processes of inhibitory interneurons in the molecular (and sometimes Purkinje cell) layer and the granule cells in the internal layer, although there were also some unusually brightly stained non-granule cells in this layer (possibly

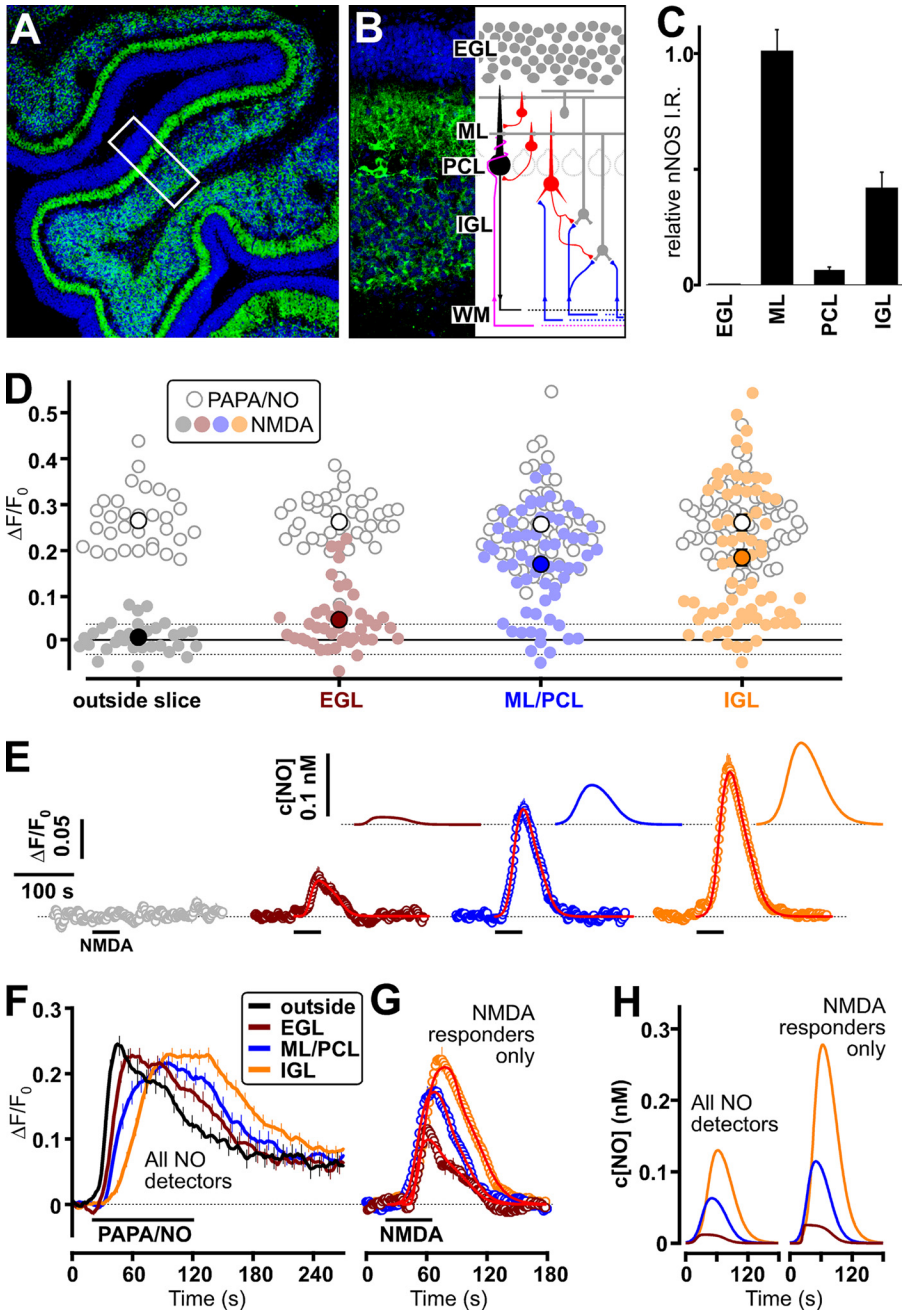

FIGURE 3. **Regional distribution of NO release in cerebellar slices and its relationship to nNOS immunostaining.** *A*, low power image of cerebellar section immunostained for nNOS (*green*). Nuclei are stained *blue*. A region is shown in *B* at a higher power (the orientation is indicated by the *rectangle* in *A*), together with a schematic showing the main constituent neurons and circuitry (*WM*, white matter; *IGL*, internal granule cell layer; *PCL*, Purkinje cell layer; *ML*, molecular layer; *EGL*, external granule cell layer). *C*, quantification of the nNOS immunoreactivity in different cerebellar layers. Three different regions, having the dimensions of the *rectangle* in *A*, were analyzed using ImageJ (http://rsbweb.nih.gov/ij/). *D*, distribution of peaks of detector cell responses to 30 μM NMDA (*filled symbols*) and 5 μM PAPA/NO (*open symbols*) outside the slices and under the different cerebellar layers (*ML/PCL* = molecular plus Purkinje cell layers) in seven experiments; *larger symbols* are mean values. *Broken horizontal lines* are ± S.D. of the baseline noise. Time courses of the mean responses are shown in *E*, with the c[NO] profiles shown in the insets. *Red lines* (main panel) are fits of the c[NO] profiles to the data. *F*, average of the responses of the same cells in *D* and *E* to PAPA/NO. *G*, mean responses of only those detector cells giving a measurable response to NMDA, the corresponding c[NO] profiles being shown in *H* (*right*) in comparison with profiles from all detector cells (*left*). For clarity, errors for every fifth point are shown in *F* and *G*. *Lines* in *G* are fits of the c[NO] profiles to the data. The *box* in *A* (expanded in *B*) is 105 × 276 μm.

migrating interneurons (28)). As expected from the *in vivo* staining (Fig. 3, *A–C*), Purkinje cells were nNOS-negative; the intermingling of their dendrites with the nNOS-positive processes of interneurons becomes evident after co-staining for the Purkinje cell marker calbindin (Fig. 5*E*).

NMDA-evoked NO Signals in Hippocampus—Similar experiments were carried out using rat hippocampus in which, as in the cerebellum, NO has been widely studied in relation to its role in synaptic plasticity (1). The recordings were centered on the cell body region of the CA1 area (Fig. 6, *A–C*) where electrode measurements had suggested the largest NMDA-evoked NO concentrations (0.3 μM) are to be found (29). Exposure to NMDA (30 μM in the presence of tetrodotoxin) produced responses in the detector cells that had similar shapes to those

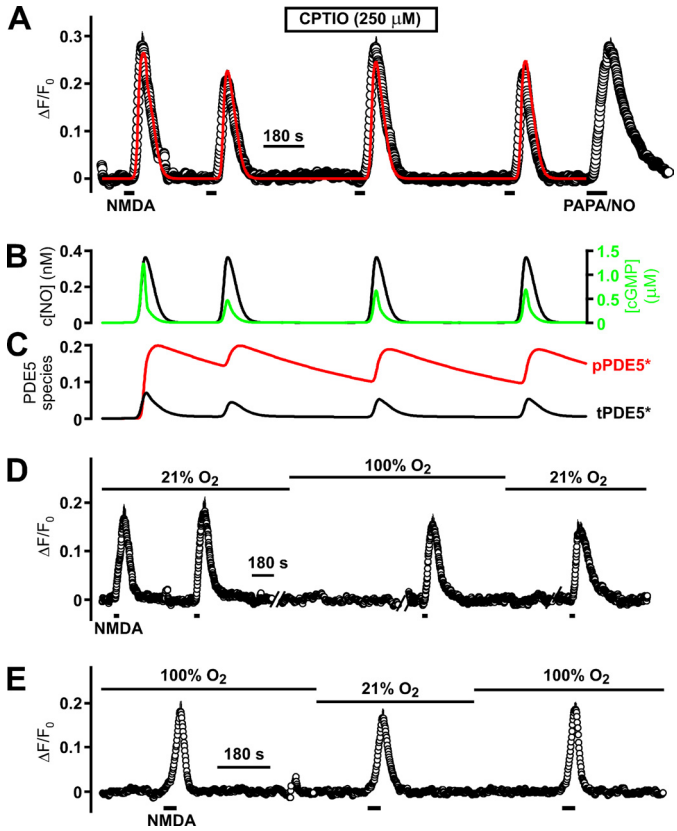

FIGURE 4. **Effect of CPTIO and O_2 on NO detector cell responses to stimulation of cerebellar slices with NMDA.** *A*, increased detector response to NMDA (30 μM, 45 s) in the presence of the NO scavenger CPTIO in one experiment. The mean change in three experiments was +12 ± 9%. As shown by the simulation (*B* and *C*) this increase can be largely explained by a diminution in the proportion of the persistently active PDE5 (*pPDE5**) after the second NMDA application, with an unaltered NO profile. *D* and *E*, detector cell responses to NMDA showed no obvious change when the superfusion solution was switched from one equilibrated with air (21% O_2) to one equilibrated with pure O_2 (*D*) or vice versa (*E*). Pure O_2 was used from the start of the experiment in *E*; *D* and *E* are separate experiments.

recorded using cerebellum and which were inhibited by L-nitroarginine (Fig. 6*D*). The average peak c[NO] fitting these responses was ~200 pM (Fig. 6*D*, *insets*). Analysis of the c[NO] values recorded in individual detector cells ($n = 14$; two experiments) suggested, again, that the data were not significantly drawn from a normally distributed population ($p = 2 \times 10^{-5}$ by the Shapiro-Wilk test). Unlike with the cerebellum, no values <100 pM were registered, although the highest one (2.4 nM) was similar. From log normal fits, the median c[NO] came to 246 pM (Table 1) and, on average, the c[NO] profiles were broader than in the cerebellum, reflecting a 2-fold slower decay during NMDA washout (Fig. 6*E*).

DISCUSSION

Since the discovery of NO as a biological messenger, there has been debate and controversy over the most basic question of what physiological or pathophysiological NO concentrations actually are. The answer has profound implications for understanding how NO operates in health and disease, and for trying to emulate endogenous NO signals experimentally. Innumerable attempts have been made to record NO levels using electrodes of various sizes and designs, but overall, the results show an irreconcilable degree of inconsistency, suggesting that factors such as cross-reactivity intrude into the measurements. The method we used here circumvents this problem because having NO receptors as the detectors ensures a high degree of specificity. The only other known ligand is carbon monoxide, which has only very low potency and efficacy (30, 31) and, as the responses we recorded were blocked by NO synthase inhibition, its contribution can be disregarded. Furthermore, the signal amplification inherent in the NO-cGMP pathway endows cells with an NO sensitivity orders of magnitude higher than is achievable with electrodes (13) and, unlike electrodes, our recording method does not consume NO.

Previous electrode recordings of evoked NO signals in the cerebellum have yielded values of between 2 nM and 2 μM (32, 33). Values of 0.12 μM (34) to 2 μM (35) were reported in the hippocampus after maximal NMDA stimulation. Our method puts the median detected values for these two brain regions at 100 and 250 pM, respectively, following half-maximal stimulation of NMDA receptors. The results are compatible with the lowest electrode recordings made in brain (55 and 400 pM in different layers of the cerebral cortex being the lowest (36)), with a failure to record NMDA-evoked NO production in cerebellum using an electrode having a detection limit of 6 nM (37), and with indirect estimates based on theoretical modeling (6), or on calibrated cGMP measurements in brain slices (7–9). An apparently single recording made near a cultured hippocampal neuron using different detector cells also suggested an NO concentration of ~100 pM (10). Thus, although very low, the NO concentrations that we detect do have independent theoretical and experimental backing.

Being small compared with the sensor area of most electrodes, the NO detector cells have also furnished a level of spatial detail not available beforehand. In the cerebellum, our finding that the internal granule cell layer gave the largest signals and the external granule cell layer the lowest signals is in good agreement with evidence based on measuring NMDA-evoked cGMP accumulation after lesioning discrete cell populations (38) and with NO synthase activity measurements in microdissected layers of the developing cerebellum (39). Overall, the molecular layer offered brighter nNOS immunostaining than the internal granule cell layer, yet, in combination with the Purkinje cell layer, gave lower c[NO]. This may relate partly to the lack of nNOS in Purkinje cells but could also reflect non-linearity between immunostaining and nNOS content as a result of epitope masking: with stronger fixation, granule cell nNOS immunostaining is diminished greatly, whereas that of the molecular layer is preserved (*cf.* Ref. 40), so that even with weak fixation, antibody binding to granule cell nNOS may be suboptimal.

Regardless of the cerebellar region, the detector cells recorded substantial variability in NO concentration. nNOS immunostaining indicated a wide size range of potential NO emitters near the slice surface. Although this microheterogeneity may contribute to the spectrum of recorded NO signals, the relative size of the detector cells would be expected to average it out. Rather, the lognormal distributions of the signal amplitudes (Fig. 5*B*) would be expected from the detectors being located at varying distances from the overlying sources, as is

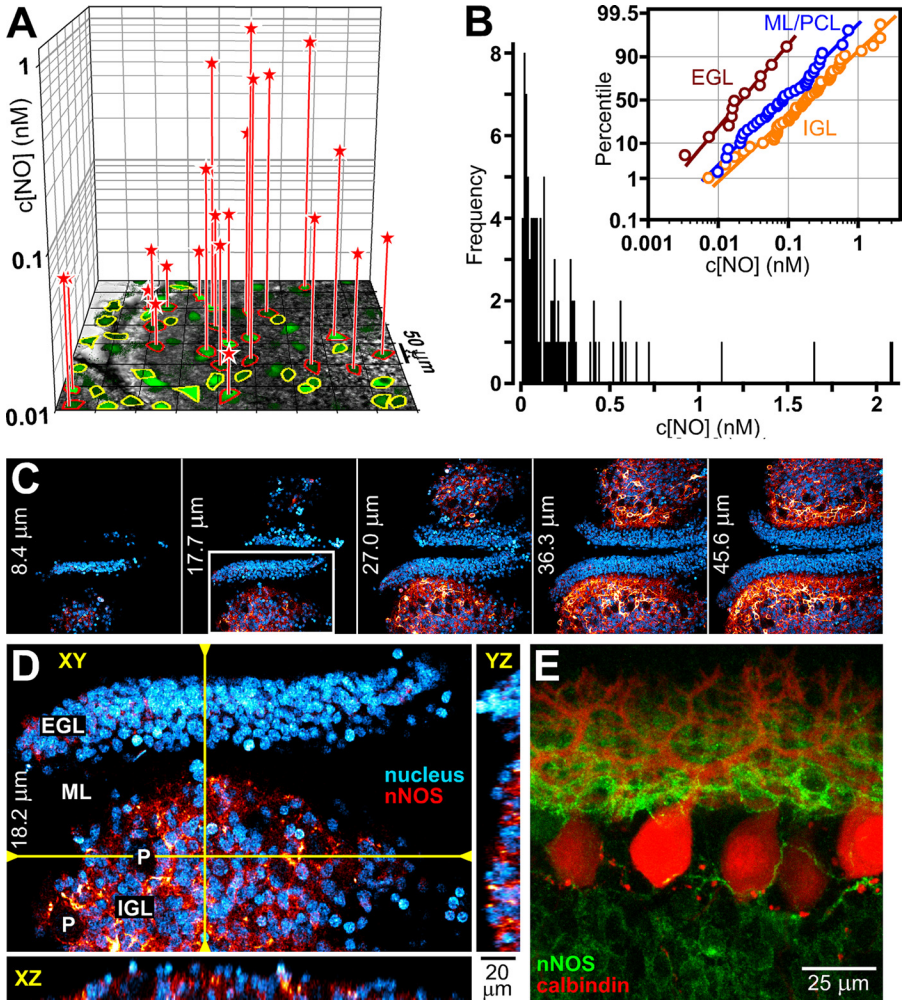

FIGURE 5. **Heterogeneity of NO sources and signals in cerebellar slices.** *A*, spread of peak c[NO] (*red stars*) registered in individual detector cells on stimulation by NMDA (30 μM, 45 s) according to their cerebellar location. Detector cells outlined in *yellow* are non-responders (but responders to PAPA/NO). *B*, skewed frequency distribution of individual peak c[NO] in responder cells in five experiments (95 cells; 10 pM bins). The data conformed to a lognormal distribution, as shown by the linear lognormal probability plots of the same data separated according to location (*inset*). For analysis of these data, see Table 1. *C*, thumbnails of nNOS immunostaining (*red glow*) in a cerebellar slice (after incubation) at the distances from the outermost plane indicated at the *left* of each frame. Nuclei are stained *cyan*. *D*, enlargement of a lobule (outlined in *C*). At the *right* and *below* are images in the z-plane at the positions of the *yellow lines*, showing nNOS staining from the slice surface inwards (*P* = Purkinje cell somata). The *scale bar* (*lower right*) applies to all planes. *E*, co-staining for nNOS (*green*) and the Purkinje cell marker, calbindin (*red*), in a cerebellar slice. *IGL*, internal granule cell layer; *PCL*, Purkinje cell layer; *ML*, molecular layer; *EGL*, external granule cell layer.

TABLE 1

Distribution of c[NO] values in cerebellar and hippocampal slices

The values are from fits of the data to lognormal distributions. σ^* is the multiplicative S.D. (50). Multiplying and dividing the median by σ^* gives the range containing 68.3% of the data (95.5% if $(\sigma^*)^2$ is used). The mode is the peak of the lognormal probability density function. Values in parentheses are from the fits shown in supplemental Fig. 4. Statistical analysis was carried out on log-transformed experimental data (all normally distributed according to the Shapiro-Wilk test) using 1-way analysis of variance followed by Tukey's test (n = number of detector cells analyzed).

Brain region	Median c[NO]	Mode c[NO]	σ^*	n	Statistics
	pM	pM			
Cerebellum (All)	102	18	3.77	95	
1. External granule cell layer	21 (23)	8.5 (8.9)	2.58 (2.63)	11	1 *versus* 2: $p = 0.0032$
2. Molecular/Purkinje cell layer	80 (81)	23 (22)	3.05 (3.13)	33	1 *versus* 3: $p < 0.0001$
3. Internal granule cell layer	171 (178)	40 (42)	3.33 (3.32)	51	2 *versus* 3: $p = 0.011$
Hippocampus (CA1)	287 (308)	140 (153)	2.33 (2.31)	14	$p = 0.006$ *versus* cerebellum

likely in any case. The distribution would arise because the logarithm of the NO concentration declines roughly in proportion to distance (supplemental Fig. 4*B*). Providing a detector cell consumes NO at only a moderate rate (0–10 s^{-1}), its intracellular NO concentration should be relatively uniform and correspond to the concentration normally found close to the position of its outermost cell membrane (supplemental Fig. 4*C*). Thus, the NO concentration recorded by a detector cell would be a function of the overlying source strength and its distance from the source. A model constructed to examine this hypothesis generated good fits to the experimental data (supplemental Fig. 4*D* and Table 1). From the fits, the recorded median values (Table 1) correspond to the NO concentrations found 4.2 ± 0.3 μm from the source surfaces, consistent with nNOS extending

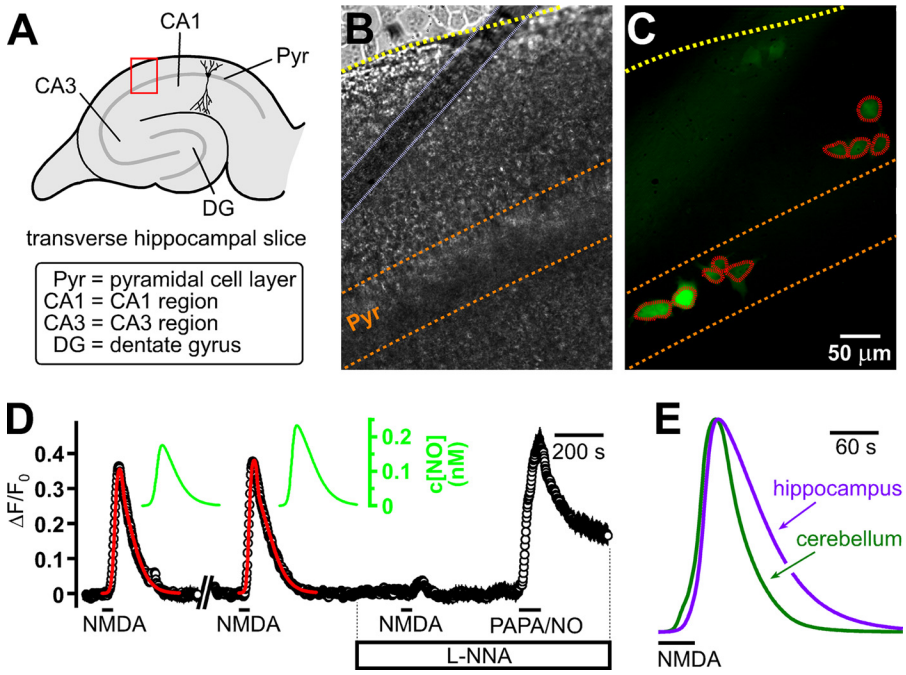

FIGURE 6. **Detection of NO from NMDA-stimulated hippocampal slices.** *A*, schematic of a hippocampal slice, indicating the region (*boxed*) shown in the brightfield (*B*) and fluorescent (*C*) experimental images. The angled structure demarcated by *dots* in *B* (fluorescing mildly in *C*) is a strand of the slice anchor. *Pyr*, pyramidal cell layer. Detector cells (*C*) are outlined in *red*. *D*, mean detector cell responses to NMDA (30 μM, 45 s) in one experiment in the absence and presence of L-nitroarginine (*L-NNA*, 30 μM), with a control application of PAPA/NO (5 μM, 90 s) at the end. *Insets* are the c[NO] profiles from the control NMDA applications; *red lines* (main panel) are their fits to the data. *E*, comparison of the mean c[NO] time courses in cerebellum *versus* hippocampus (normalized to the maxima); the times for 50% decay from the peak were 31 s (cerebellum; $n = 95$; five experiments) and 60 s (hippocampus; $n = 14$; two experiments).

TABLE 2
Parameters simulating the c[NO] distributions recorded by detector cells

Region	Maximum source surface-to-detector cell separation	NO concentration at source surface	NO emission rate at source surface	Tissue NO source strength[a]	Half-maximum NO synthase enzyme activity[b]
	μm	*nM*	*nmol m^{-2} s^{-1}*	*nM s^{-1}*	*nM s^{-1}*
Cerebellum					158 (whole cerebellum)
IGL[c]	9.5	1.4	1.0	353 (3.1 nM)	
ML/PCL	9.0	0.57	0.41	160 (1.2 nM)	
EGL	8.0	0.12	0.088	36 (0.25 nM)	
Hippocampus (CA1)	7.0	1.4	1.0	353 (3.1 nM)	139 (whole hippocampus)

[a] Tissue NO generation rates giving the concentrations at the source surface (third column). Values in parentheses are the predicted steady-state NO concentrations within the tissue. See supplemental Methods for details of the calculations.
[b] From assays on homogenized adult rat cerebellum and hippocampus (51), assuming 1 ml/g wet weight and age corrections from data on rat cerebellum and forebrain, respectively (52).
[c] IGL, internal granule cell layer; EGL, external granule cell layer; ML/PCL, molecular/Purkinje cell layer.

out to the slice surface (Fig. 5*D* and supplemental Movie 2) and the detector cells being located just below it. The fits further indicate that the NO concentrations at the source surfaces are close to the maximum values recorded experimentally. The rates of NO production within the tissue giving rise to the surface concentrations are calculated as 36–353 nM/s, and the tissue NO concentrations 250 pM to 3 nM depending on region (Table 2).

It should be noted that some uncertainty exists about the precise value of one of the model parameters, namely the rate of inactivation of NO (19, 37), but this parameter has little influence on the NO concentrations deduced for the source surface or its core, although it will affect the NO synthesis rates needed to sustain these concentrations (supplemental Methods). With the inactivation rate estimated for cerebellar slices (150 s^{-1}) (19), however, the deduced synthesis rates do broadly agree with nNOS activity measurements in homogenates of cerebellum and hippocampus, assuming the EC_{50} NMDA concentration used experimentally gives half-maximal nNOS activity (Table 2). If NMDA receptors and nNOS are mainly co-localized in synapses (41) and the cerebellar internal granule cell layer in our experiments has a density of synapses similar to this region of the 21-day-old rat (1 synapse/μm^3) (42), each with 40 NMDA receptors (43) and associated nNOS molecules, the deduced source strength for this layer (353 nM/s; Table 2) corresponds to each active nNOS generating 10 NO molecules/s. This rate is similar to that predicted for nNOS from enzyme studies (27, 44), although it is not known that the NO sources in our experiments are purely synaptic. Nonetheless, assuming this rate of synthesis to be approximately correct and that, physiologically, ~10% of synaptic NMDA receptors are active (45), source NO concentrations at the level of a single synapse would be in the 10–100 pM range (supplemental Fig. 4*A*), perhaps a few-fold higher during the initial burst phase of NO synthesis (27, 44). With the NO receptors situated close by, as is predicted for the α2β1 subtype that is abundant in brain (46),

signals of this amplitude are likely to be functionally transmissible.

The results provide a quantitatively coherent link between the NO concentrations that receptive cells are tuned to detect, the concentrations that are expected to exist based on nNOS localization and enzymology, and the concentrations found after evoking endogenous NO production from nNOS. At these concentrations, no target for NO other than its receptors has been identified, and its influence on mitochondrial cytochrome *c* oxidase would be negligible, in line with experimental evidence (37, 47). Despite a diffusion-limited reaction of NO with superoxide anions forming peroxynitrite (48), the rate of this reaction at 100 pM NO will be slow (1–2 s^{-1}). Hence, NO appears to have evolved to operate as a transmitter at concentrations well below those having other effects and is able to do so because of the special transduction properties of its enzyme-linked receptors. If, when, and how NO from nNOS rises to toxic concentrations in the brain, as is presumed to happen in some neurodegenerative disorders (49), remain open questions.

Acknowledgments—We are grateful to Professor Doris Koesling (Bochum, Germany) for generously supplying the GC/PDE HEK 293T cell line used in this work.

REFERENCES

1. Garthwaite, J. (2008) *Eur. J. Neurosci.* **27,** 2783–2802
2. Knowles, R. G., and Moncada, S. (1992) *Trends Biochem. Sci.* **17,** 399–402
3. Rand, M. J., and Li, C. G. (1995) *Annu. Rev. Physiol.* **57,** 659–682
4. Ignarro, L. J. (1991) *Biochem. Pharmacol.* **41,** 485–490
5. Murad, F. (1994) *Recent Prog. Horm. Res.* **49,** 239–248
6. Hall, C. N., and Garthwaite, J. (2009) *Nitric Oxide* **21,** 92–103
7. Bellamy, T. C., Griffiths, C., and Garthwaite, J. (2002) *J. Biol. Chem.* **277,** 31801–31807
8. Griffiths, C., Garthwaite, G., Goodwin, D. A., and Garthwaite, J. (2002) *Eur. J. Neurosci.* **15,** 962–968
9. Keynes, R. G., Duport, S., and Garthwaite, J. (2004) *Eur. J. Neurosci.* **19,** 1163–1173
10. Sato, M., Nakajima, T., Goto, M., and Umezawa, Y. (2006) *Anal. Chem.* **78,** 8175–8182
11. Thomas, D. D., Ridnour, L. A., Isenberg, J. S., Flores-Santana, W., Switzer, C. H., Donzelli, S., Hussain, P., Vecoli, C., Paolocci, N., Ambs, S., Colton, C. A., Harris, C. C., Roberts, D. D., and Wink, D. A. (2008) *Free Radic. Biol. Med.* **45,** 18–31
12. Halvey, E. J., Vernon, J., Roy, B., and Garthwaite, J. (2009) *J. Biol. Chem.* **284,** 25630–25641
13. Batchelor, A. M., Bartus, K., Reynell, C., Constantinou, S., Halvey, E. J., Held, K. F., Dostmann, W. R., Vernon, J., and Garthwaite, J. (2010) *Proc. Natl. Acad. Sci. U.S.A.* **107,** 22060–22065
14. Garthwaite, J., Charles, S. L., and Chess-Williams, R. (1988) *Nature* **336,** 385–388
15. Nausch, L. W., Ledoux, J., Bonev, A. D., Nelson, M. T., and Dostmann, W. R. (2008) *Proc. Natl. Acad. Sci. U.S.A.* **105,** 365–370
16. Mullershausen, F., Russwurm, M., Koesling, D., and Friebe, A. (2004) *Mol. Biol. Cell* **15,** 4023–4030
17. Salter, M., Duffy, C., Garthwaite, J., and Strijbos, P. J. (1996) *J. Neurochem.* **66,** 1683–1690
18. Southam, E., East, S. J., and Garthwaite, J. (1991) *J. Neurochem.* **56,** 2072–2081
19. Hall, C. N., and Garthwaite, J. (2006) *J. Physiol.* **577,** 549–567
20. Roy, B., Halvey, E. J., and Garthwaite, J. (2008) *J. Biol. Chem.* **283,** 18841–18851
21. Glitsch, M., and Marty, A. (1999) *J. Neurosci.* **19,** 511–519
22. Bredt, D. S., and Snyder, S. H. (1994) *Neuron.* **13,** 301–313
23. Griffiths, C., Wykes, V., Bellamy, T. C., and Garthwaite, J. (2003) *Mol. Pharmacol.* **64,** 1349–1356
24. Gardner, P. R., Martin, L. A., Hall, D., and Gardner, A. M. (2001) *Free Radic. Biol. Med.* **31,** 191–204
25. Liu, X., Srinivasan, P., Collard, E., Grajdeanu, P., Lok, K., Boyle, S. E., Friedman, A., and Zweier, J. L. (2010) *Free Radic. Biol. Med.* **48,** 554–559
26. Thomas, D. D., Liu, X., Kantrow, S. P., and Lancaster, J. R., Jr. (2001) *Proc. Natl. Acad. Sci. U.S.A.* **98,** 355–360
27. Santolini, J., Adak, S., Curran, C. M., and Stuehr, D. J. (2001) *J. Biol. Chem.* **276,** 1233–1243
28. Zhang, L., and Goldman, J. E. (1996) *Neuron* **16,** 47–54
29. Ledo, A., Barbosa, R. M., Gerhardt, G. A., Cadenas, E., and Laranjinha, J. (2005) *Proc. Natl. Acad. Sci. U.S.A.* **102,** 17483–17488
30. Sato, M., Hida, N., and Umezawa, Y. (2005) *Proc. Natl. Acad. Sci. U.S.A.* **102,** 14515–14520
31. Stone, J. R., and Marletta, M. A. (1994) *Biochemistry* **33,** 5636–5640
32. Amatore, C., Arbault, S., Bouret, Y., Cauli, B., Guille, M., Rancillac, A., and Rossier, J. (2006) *Chemphyschem.* **7,** 181–187
33. Kimura, S., Uchiyama, S., Takahashi, H. E., and Shibuki, K. (1998) *J. Neurosci.* **18,** 8551–8558
34. Frade, J. G., Barbosa, R. M., and Laranjinha, J. (2009) *Hippocampus* **19,** 603–611
35. Lourenço, C. F., Santos, R., Barbosa, R. M., Gerhardt, G., Cadenas, E., and Laranjinha, J. (2011) *Hippocampus* **21,** 622–630
36. Wakatsuki, H., Gomi, H., Kudoh, M., Kimura, S., Takahashi, K., Takeda, M., and Shibuki, K. (1998) *J. Physiol. Lond.* **513,** 71–81
37. Hall, C. N., and Attwell, D. (2008) *J. Physiol* **586,** 3597–3615
38. Garthwaite, J., and Garthwaite, G. (1987) *J. Neurochem.* **48,** 29–39
39. Wang, W., Nakayama, T., Inoue, N., and Kato, T. (1998) *Brain Res. Dev. Brain Res.* **111,** 65–75
40. Burette, A., Zabel, U., Weinberg, R. J., Schmidt, H. H., and Valtschanoff, J. G. (2002) *J. Neurosci.* **22,** 8961–8970
41. Valtschanoff, J. G., and Weinberg, R. J. (2001) *J. Neurosci.* **21,** 1211–1217
42. Warren, M. A., and Bedi, K. S. (1990) *J. Anat.* **170,** 173–182
43. Kennedy, M. B. (2000) *Science* **290,** 750–754
44. Salerno, J. C. (2008) *FEBS Lett.* **582,** 1395–1399
45. Zeng, S., and Holmes, W. R. (2010) *J. Neurophysiol.* **103,** 1798–1808
46. Mergia, E., Russwurm, M., Zoidl, G., and Koesling, D. (2003) *Cell Signal.* **15,** 189–195
47. De Visscher, G., Springett, R., Delpy, D. T., Van Reempts, J., Borgers, M., and van Rossem, K. (2002) *J. Cereb. Blood Flow Metab.* **22,** 515–519
48. Ferrer-Sueta, G., and Radi, R. (2009) *ACS Chem. Biol.* **4,** 161–177
49. Brown, G. C. (2010) *Nitric Oxide.* **23,** 153–165
50. Limpert, E., Stahel, W. A., and Abbt, M. (2001) *Bioscience* **51,** 341–352
51. Salter, M., Duffy, C., Garthwaite, J., and Strijbos, P. J. (1995) *Neuropharmacology.* **34,** 639–649
52. Lizasoain, I., Weiner, C. P., Knowles, R. G., and Moncada, S. (1996) *Pediatr. Res.* **39,** 779–783